J Electroceram (2008) 21:72–77
DOI 10.1007/s10832-007-9079-5

Epitaxial growth of multilayered $(Bi,La)_4Ti_3O_{12}/Pb(Zr,Ti)O_3$ ferroelectric thin films with different orientations

Dinghua Bao · Xinhua Zhu · Marin Alexe · Dietrich Hesse

Published online: 29 March 2007

Abstract Epitaxial $(Bi,La)_4Ti_3O_{12}$ (BLT) thin films, epitaxial $Pb(Zr,Ti)O_3$ (PZT) thin films, and epitaxial multilayered BLT/PZT ferroelectric thin films with different orientations were prepared on $SrTiO_3$ (STO) single crystal substrates by pulsed laser deposition. From X-ray pole-figures and electron diffraction patterns, the epitaxial orientation relationships between BLT layers, PZT layers, and STO substrates were identified to be (1) BLT(001)// PZT(001)//STO(001), and BLT[110]//PZT[100]//STO[100] for the multilayered thin films on (001)-oriented STO substrates, and (2) BLT(118)//PZT(011)//STO(011), and $BLT\left[\bar{1}\,\bar{1}0\right]//PZT[100]//SrTiO_3[100]$ for the multilayered films on (011)-oriented STO substrates. Tri-layered films of the same compositions showed well-defined hysteresis loops as well as a high fatigue resistance up to 1×10^{10} switching cycles.

Keywords Multilayered film · Ferroelectric · Epitaxial · Orientation

D. Bao (✉)
State Key Laboratory of Optoelectronic Materials and Technologies, School of Physics and Engineering, Sun Yat-Sen University,
Guangzhou 510275, People's Republic of China
e-mail: stsbdh@mail.sysu.edu.cn

X. Zhu · M. Alexe · D. Hesse
Max-Planck Institute of Microstructure Physics,
Weinberg 2,
06120 Halle (Saale), Germany

1 Introduction

Perovskite dielectric/ferroelectric oxide thin films have been attractive for their applications in microelectronic and optoelectronic devices. Recently, multilayered dielectric/ferroelectric oxide thin films and superlattices have been investigated for enhanced electrical properties or new physical effects [1–3]. It has been reported that some dielectric/ferroelectric multilayered thin films and superlatttices exhibited superior electrical properties such as high dielectric constant and polarization [4, 5]. Up to now, most of the multilayered films and superlattices reported, to our knowledge, consist of components having almost the same simple perovskite structure such as $BaTiO_3/SrTiO_3$, $PbTiO_3/PbZrO_3$, and $SrTiO_3/PbTiO_3$, whereas studies on multilayered ferroelectric thin films composed of film layers having different crystallographic systems, such as simple perovskite structure and bismuth layered perovskite structure, are lacking [6, 7]. This motivated us to carry out fundamental research on multilayered thin films composed of $Pb(Zr,Ti)O_3$ (PZT) and $(Bi,La)_4Ti_3O_{12}$ (BLT). PZT and BLT have a simple perovskite structure and a bismuth layered perovskite structure, respectively. Both of them are important ferroelectric thin film materials, especially for memory applications [8, 9]. In addition, it can be found, by comparison, that their electrical properties are complementary. For example, PZT exhibits a high remanent polarization, but has poor fatigue properties on Pt electrodes [10, 11]. In contrast, BLT has a high resistance against polarization fatigue, but relatively low remanent polarization [12, 13]. Therefore, it is of considerable interest to investigate microstructure and properties of this kind of multilayered thin films.

In this study, epitaxial multilayered BLT/PZT thin films were prepared on $SrTiO_3$ (STO) substrates with different

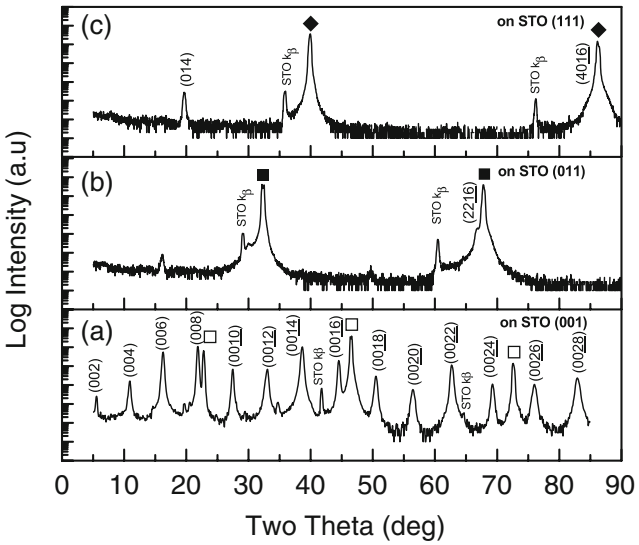

Fig. 1 XRD $\theta-2\theta$ scans of BLT thin films on (**a**) (001)-oriented, (**b**) (011)-oriented, and (**c**) (111)-oriented $SrTiO_3$ single crystal substrates

orientations by pulsed laser deposition, and their epitaxial orientation relationships and ferroelectric properties have been studied.

2 Experimental procedure

The BLT and PZT film layers were prepared on STO substrates by PLD using a KrF excimer laser (λ=248 nm) and ceramic targets of $(Bi_{3.25}La_{0.75})Ti_3O_{12}$ and $Pb_{1.3}(Zr_{0.4}Ti_{0.6})O_3$. The substrates were placed parallel to the targets at a distance of 4.5 cm. The substrate temperature and oxygen pressure were kept at 650 °C and 0.4 mbar, respectively, for the growth of BLT and PZT layers. After deposition of all the layers, the BLT/PZT samples were cooled down to room temperature at an oxygen pressure of 0.4 mbar to prevent losses of bismuth and lead.

The crystallographic orientation and epitaxial relationships of the single thin films and multilayered thin films were characterized by X-ray diffraction (XRD) $\theta-2\theta$ scans and pole figure measurements using a Philips X'Pert MRD 4-circle diffractometer with Cu K_α radiation. A Digital Instruments D5000 atomic force microscope was used for the characterization of the surface morphology. Electron diffraction patterns and transmission electron microscope (TEM) images were recorded in a Philips CM20T electron microscope operated at 200 kV. The polarization versus electric field properties of tri-layered films having the same compositions on $SrRuO_3$/STO substrates were measured by a TF 2000 ferroelectric tester (AixACCT) at a frequency of 100 Hz.

3 Results and discussion

3.1 Epitaxial BLT thin films with different orientations

Figure 1 shows XRD $\theta-2\theta$ scans (from 5 to 85°) of BLT thin films on (a) (001)-oriented, (b) (011)-oriented, and (c) (111)-oriented $SrTiO_3$ single crystal substrates. Only (*00l*) reflections of BLT and STO were observed in Fig. 1(a), indicating that BLT films are (001) oriented. Figure 1(b) indicates that BLT films are (*118*) oriented since only the (*2216*) reflection of BLT was observed. From Fig. 1(c), it can be concluded that BLT films are (104) oriented on (111)-oriented STO substrates since only the (014) and (40*16*) reflections of BLT were observed. Similar results have been reported for $(Bi,Nd)_4Ti_3O_{12}$ films [14]. The lattice mismatches between BLT and STO can be calculated in a similar way as Lee and coworkers reported for epitaxial $SrBi_2Ta_2O_9$ thin films on STO substrates [15]. The *a*-axis and *b*-axis lattice constants of BLT are about 0.545 and 0.541 nm, respectively; and the STO has a lattice constant of 0.3905 nm. For the (001)-oriented BLT film, the lattice mismatches $(d_{film}-d_{sub})/d_{sub}$ between the d spacing of BLT [100] and STO[110] and BLT[010]//STO$[\bar{1}10]$ are about −1.2 and −2%, respectively. Thus, an in-plane 45° rotation of the lattice is expected, which leads to highly *c*-axis oriented growth of BLT on (001)-oriented STO substrates. Similarly, for the BLT film on (011)-oriented STO, the two mismatch

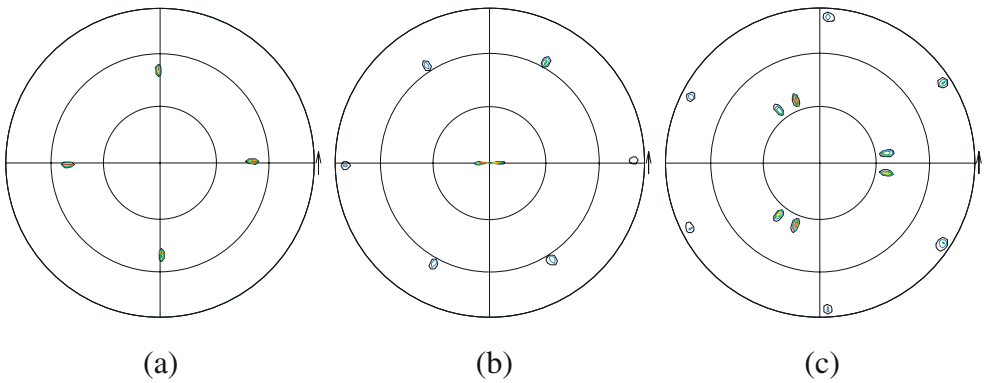

Fig. 2 X-ray pole figures of BLT thin films on (**a**) a (001)-oriented $SrTiO_3$ substrate, (**b**) a (011)-oriented $SrTiO_3$ substrate, and (**c**) a (111)-oriented $SrTiO_3$ substrate, measured at a 2θ angle corresponding to the BLT {117} planes

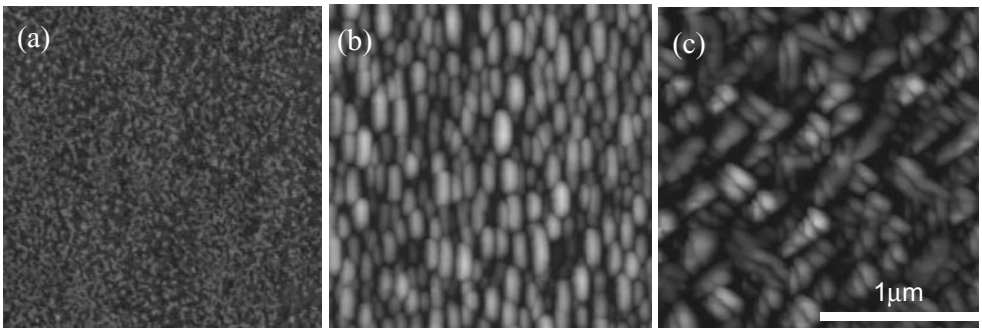

Fig. 3 AFM images of BLT thin films on (**a**) a (001)-oriented $SrTiO_3$ substrate, (**b**) a (011)-oriented $SrTiO_3$ substrate, and (**c**) a (111)-oriented $SrTiO_3$ substrate

values along STO [100] and STO $[0\bar{1}1]$ directions are −1.68 and 1.45%, respectively. For the situation of the film on (111)-oriented STO, the two mismatch values along STO [112] and STO $[1\bar{1}0]$ directions are 2.99 and −2 %, respectively.

Figure 2(a), (b), and (c) show three pole figures of BLT thin films on STO substrates with different orientations, measured at a 2θ angle corresponding to the BLT{117} planes, respectively. As can be seen in Fig. 2(a), four diffraction peaks at $\psi \approx 50°$ with 90° intervals show a four-fold symmetry from the BLT {117} poles, indicating that BLT layers had a very good in-plane orientation [16]. Note that BLT{117} planes have a tilt angle of 50.5° with respect to the BLT(001) plane which is parallel to the substrate surface. In Fig. 2(b), there are two sets of three peaks at $\psi \approx 5°$, $\psi \approx 63°$, and $\psi \approx 84°$, corresponding to (117), $(\bar{1}17)/(1\bar{1}7)$, and $(\bar{1}\,\bar{1}7)$ reflections of BLT, respectively. The two sets of peaks indicate the presence of double-twin as reported previously for epitaxial BLT films on STO substrate, and the BLT (118) plane is parallel to the substrate surface [17]. For the (104)-oriented film, there are three sets of two peaks at $\psi \approx 36°$, and $\psi \approx 84°$, the peak at $\psi \approx 36°$ corresponds to (117) and $(1\bar{1}7)$, and the other peak at $\psi \approx 84°$ to $(11\bar{7})$ and $(\bar{1}\,\bar{1}7)$ reflections of BLT, respectively, confirming a triple-domain situation and the BLT (104) plane is parallel to the substrate surface [18].

Therefore, the epitaxial relationships of BLT thin films on STO substrates having different orientations can be determined as follows:

For the BLT film on (001) STO substrate,
BLT(001)//$SrTiO_3$(001); BLT$[1\bar{1}0]$//$SrTiO_3$[100]

For the BLT film on (011) STO substrate,
BLT(118)//$SrTiO_3$(011); BLT$[\bar{1}\,\bar{1}0]$//$SrTiO_3$[100]

For the BLT film on (111) STO substrate,
BLT(104)//$SrTiO_3$(111); BLT[010]//$SrTiO_3$$[1\bar{1}0]$

Figure 3(a), (b), and (c) show three AFM images of BLT thin films on STO substrates with different orientations, respectively. It can be found that the surface morphologies and roughness are largely dependent on the orientations of the films. The (118)- and (104)- oriented films show double-twin and triple-twin structure features, respectively. That is, the (118)-oriented BLT film shows rod-shaped grains arranged mostly along one direction, and the (104)-oriented film has the grains oriented along three directions separated by 120° for each other. In addition, the (001) oriented film is most smooth, and the (104)-oriented film is most rough among the three films with different orientations. Considering that the aim of this study is to obtain multilayered thin films, small surface roughness is needed. Therefore, (001)

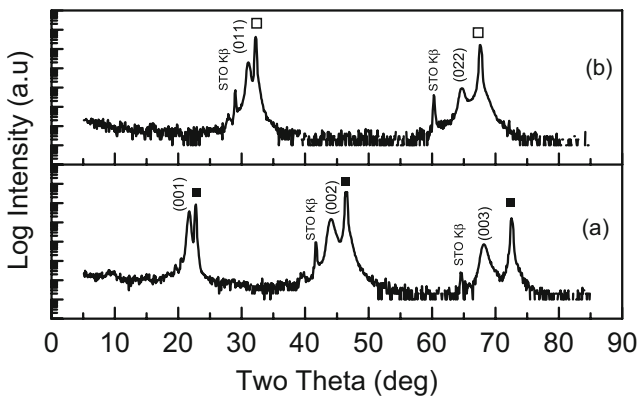

Fig. 4 X-ray $\theta-2\theta$ diffraction patterns of (**a**) PZT thin film on a (001)-oriented $SrTiO_3$ substrate, and (**b**) PZT thin film on a (011)-oriented $SrTiO_3$ substrate

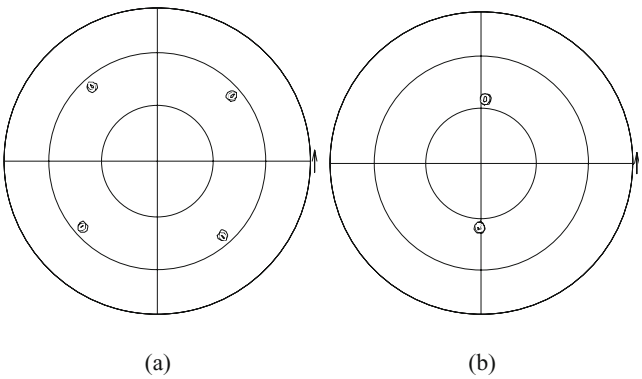

Fig. 5 X-ray pole figures of (**a**) PZT thin film on a (001)-oriented $SrTiO_3$ substrate, and (**b**) PZT thin film on a (011)-oriented $SrTiO_3$ substrate, measured at different 2θ angles, corresponding to the PZT {101} and PZT{111} planes, respectively

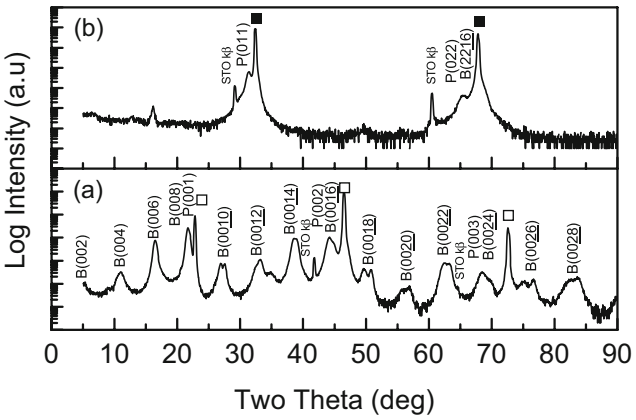

Fig. 6 XRD $\theta-2\theta$ scans of BLT/PZT multilayered thin films deposited on (**a**) (001)-oriented and (**b**) (011)-oriented $SrTiO_3$ single crystal substrates. The peaks labeled (*P*), (*B*), (*empty square*, *filled square*) are diffraction peaks from PZT Cu-$K_{\alpha1}$, BLT Cu-$K_{\alpha1}$, and STO Cu-$K_{\alpha1}$, respectively

and (011)-oriented STO substrates were selected to prepare multilayered thin films.

3.2 Epitaxial PZT thin films with different orientations

Figure 4 shows XRD $\theta-2\theta$ scans (from 5 to 85°) of PZT thin films deposited on (a) (001)-oriented and (b) (011)-oriented $SrTiO_3$ single crystal substrates, respectively. PZT has similar structure and a very small lattice mismatch with STO. Therefore, PZT grows with *c*-axis orientation on (001) STO substrate and with (011) orientation on (011) STO substrate as shown in Fig. 4.

Figure 5(a) and (b) show two pole figures of PZT thin films on (001)- and (011)-oriented STO substrates, measured at different 2θ angles, corresponding to the PZT{101} and PZT{111} planes, respectively. In Fig. 5(a) four diffraction peaks at $\psi\approx45°$ indicate a four-fold symmetry from the PZT {101} poles without satellites, demonstrating that the PZT film has a good in-plane orientation. From Fig. 5(b), it can be seen that there are two peaks at $\psi\approx35°$, corresponding to

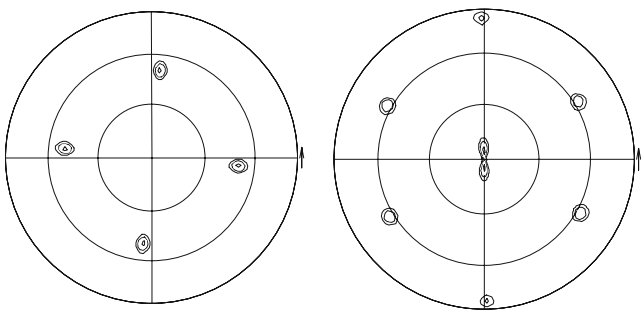

Fig. 7 X-ray pole figures of BLT/PZT multilayered thin films on (**a**) (001)-oriented and (**b**) (011)-oriented STO substrates, measured at the 2θ angle corresponding to the BLT{117} planes

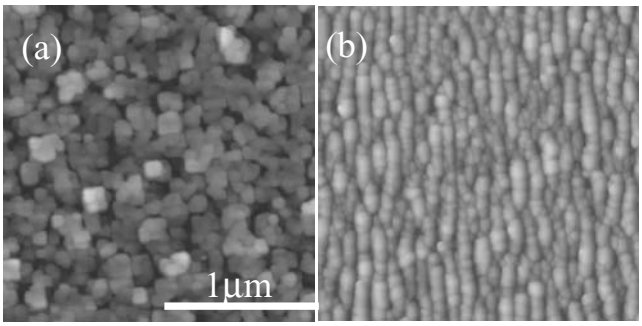

Fig. 8 AFM images of the surface morphologies of BLT/PZT multilayered thin films deposited on (**a**) a (001)-oriented and (**b**) (011)-oriented $SrTiO_3$ single crystal substrates

(111) PZT reflections, indicating the epitaxial growth of the PZT film with two in-plane orientations with 180° symmetry. The two peaks also indicate that the PZT (011) planes are parallel to the (011) STO substrate surface.

Thus, the epitaxial relationships of PZT thin films on STO substrates were determined as follows:

For PZT film on (001) STO substrate,
$PZT(001)//SrTiO_3(001)$; $PZT[100]//SrTiO_3[100]$

For PZT film on (011) STO substrate,
$PZT(011)//SrTiO_3(011)$; $PZT[100]//SrTiO_3[100]$

3.3 Epitaxial multilayered BLT/PZT thin films with different orientations

Figure 6 shows XRD $\theta-2\theta$ scans of BLT/PZT multilayered thin films deposited on (a) (001)-oriented and (b) (011)-oriented $SrTiO_3$ single crystal substrates. It can be seen from Fig. 6(a) that only the (*00l*) reflections of PZT, BLT, and STO are observed, indicating that all of the PZT and BLT layers are (001) oriented on the (001)-oriented $SrTiO_3$ substrate. As mentioned before, BLT has *a*-axis and *b*-axis lattice constants of about 0.545 and 0.541 nm, respectively, both of which are very close to the diagonal distance of STO along the [110] direction (0.552 nm). In addition, PZT has a similar structure and very small lattice mismatch with STO. The diagonal distance of PZT along the [110] direction is about 0.563 nm, which is also close to the *a*-axis and *b*-axis lattice constants of BLT. Therefore, BLT

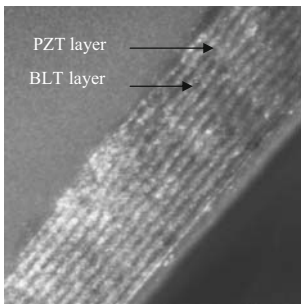

Fig. 9 TEM cross-section image of a BLT/PZT multilayered thin film deposited on (001)-oriented $SrTiO_3$ single crystal substrate

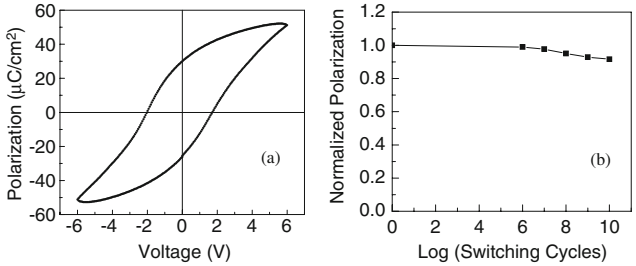

Fig. 10 P-E hysteresis loop (**a**) and fatigue curve (**b**) of a BLT/PZT/BLT trilayered thin film deposited on (011)-oriented $SrRuO_3$ covered $SrTiO_3$ substrates

and PZT layers can alternatively be grown on STO substrates with good epitaxial orientation. In Fig. 6(b), only the (011) and (022) peaks of PZT and STO, and the (22*16*) peak of BLT are observed, indicating that the PZT layers showed a (011) orientation and that the BLT layers were (118) oriented, and also confirming the alternative growth of BLT and PZT layers on the (011) STO substrate with good epitaxial orientation.

Figure 7 shows two pole figures of BLT/PZT multilayered thin films on (a) (001)-oriented and (b) (011)-oriented STO substrates, measured at the 2θ angle corresponding to the BLT{117} planes. Comparing Fig. 7(a) with Fig. 2(a), and Fig. 7(b) with Fig. 2(b), respectively, it can be found that the BLT layers in the multilayered structure have the same in-plane orientation alignments as the individual BLT thin films. Similarly, the PZT layers in the multilayered films have the same in-plane orientation alignments as the individual PZT thin films.

Therefore, the epitaxial relationships of the multilayered thin films on the (001) STO substrates can be written as follows:

BLT(001)//PZT (001)//STO (001), and BLT[110]//PZT [100]//STO [100].

The epitaxial relationships of the multilayered thin films on the (011) STO substrates can be written as follows:

BLT(118)//PZT(011)//$SrTiO_3$(011); BLT$[\bar{1}\,\bar{1}0]$//PZT [100]//$SrTiO_3$[100].

Figure 8 shows AFM images of the surface morphologies of BLT/PZT multilayered thin films deposited on (a) a (001)-oriented and (b) a (011)-oriented $SrTiO_3$ single crystal substrate. Homogeneous sub-micron grain size, and low surface roughness are observed for the multilayered thin film on (001)-oriented $SrTiO_3$ substrate. For the multilayered thin film on (011)-oriented $SrTiO_3$ substrate, the (118)-oriented upper BLT layer shows rod-shaped grains arranged mostly along one direction. This is similar to that of an epitaxial (118)-oriented single BLT thin film although the aspect ratios are somewhat different. In addition, from AFM images, it can be observed that the surface roughness of the multilayered film on (001) STO substrate is much lower than that of the multilayered film on (011) STO substrate.

Figure 9 shows a TEM cross-section image of a BLT/PZT multilayered thin film deposited on (001)-oriented $SrTiO_3$ single crystal substrate. It is observed that the multilayered film has a planar, sharp BLT/STO interface and smooth BLT/PZT interfaces.

Investigations of the ferroelecectric properties of the multilayered films are in progress. So far, ferroelectric properties of all-epitaxial tri-layered BLT/PZT/BLT thin films on SRO-covered (001)- and (011)-oriented STO substrates have been determined [6, 7]. The remanent polarization and coercive field were 13.9 μC/cm^2 and 72.9 kV/cm, respectively, for the tri-layered thin films on (001) STO substrates, and 28.1 μC/cm^2 and 33.7 kV/cm, respectively, for the tri-layered thin films on (011) STO substrates. Both of these thin films showed a high fatigue resistance at least up to 10^{10} switching pulse cycles. Figure 10 shows typical hysteresis loop (a) and fatigue curve (b) of a Pt/BLT/PZT/BLT/SRO capacitor on (011)-oriented STO substrate, respectively. Good ferroelectric properties and high fatigue resistance have been confirmed in these multilayered structures.

4 Conclusions

Epitaxial $Bi_{3.25}La_{0.75}Ti_3O_{12}/Pb(Zr_{0.4}Ti_{0.6})O_3$ multilayered ferroelectric films were prepared on $SrTiO_3$ substrates with different orientations by pulsed laser deposition. The epitaxial relationships between BLT layers, PZT layer, and $SrTiO_3$ substrate were identified to be (1) BLT(001)//PZT (001)//STO (001), and BLT[110]//PZT [100]//STO [100] for the multilayered thin films on the (001) STO substrates, and (2) BLT(118)//PZT(011)//$SrTiO_3$(011); BLT$[\bar{1}\,\bar{1}0]$//PZT[100]//$SrTiO_3$[100] for the multilayered thin films on the (011) STO substrates. Studies of the ferroelectric properties of the multilayered films are in progress. Tri-layered films of the same compositions showed well-defined hysteresis loops as well as a high fatigue resistance up to 1×10^{10} switching cycles.

Acknowledgments This work was financially supported by DFG via the Group of Researches FOR 404 at Martin-Luther-Universität Halle-Wittenberg. D.H. Bao and X.H. Zhu gratefully acknowledge support from the Alexander von Humboldt Foundation, Germany. D. H.Bao also acknowledges support from NSFC (No. 10574164 & No. U0634006), FANEDD (No.200441), and the project-sponsored by Guangzhou Science and Technology Bureau (No. 2005J1-C0031).

References

1. L. Kim, D. Jung, J. Kim, Y.S. Kim, J. Lee, Appl. Phys. Lett. **82**, 2118 (2003)

2. J.C. Jiang, X.Q. Pan, W. Tian, C.D. Theis, D.G. Schlom, Appl. Phys. Lett. **74**, 2851 (1999)
3. J.B. Neaton, K.M. Rabe, Appl. Phys. Lett. **82**, 1586 (2003)
4. T. Tsurumi, I. Ichikawa, T. Harigai, H. Kakemoto, J. Appl. Physi. **91**, 2284 (2002)
5. H.N. Lee, H.M. Christen, M.F. Chisholm, C.M. Roulean, D.H. Lowndes, Nature (Lond.) **433**, 395 (2005)
6. D.H. Bao, S.K. Lee, X.H. Zhu, M. Alexe, D. Hesse, Appl. Phys. Lett. **86**, 082906 (2005)
7. D.H. Bao, X.H. Zhu, M. Alexe, D. Hesse, J. Appl. Physi. **98**, 014101 (2005)
8. J.F. Scott, C.A. Paz de Araujo, Science **246**, 1400 (1989)
9. B.H. Park, B.S. Kang, S.D. Bu, T.W. Noh, J. Lee, W. Jo, Nature (Lond.) **401**, 682 (1999)
10. O. Auciello, J.F. Scott, R. Ramesh, Phys. Today **51**, 22 (1998)
11. D.H. Bao, N. Wakiya, K. Shinozaki, N. Mizutani, X. Yao, J. Appl. Physi. **90**, 506 (2001)
12. H.N. Lee, D. Hesse, N. Zakharov, U. Gösele, Science **296**, 2006 (2002)
13. D.H. Bao, T.W. Chiu, N. Wakiya, K. Shinozaki, N. Mizutani, J. Appl. Physi. **93**, 497 (2003)
14. A. Garg, A. Snedden, P. Lightfoot, J.F. Scott, X. Hu, Z.H. Barber, J. Appl. Physi. **96**, 3408 (2004)
15. H.N. Lee, A. Visinoiu, S. Senz, C. Hamagea, A. Pignolet, D. Hesse, U. Gosele, J. Appl Physi. **88**, 6658 (2000)
16. T. Watanabe, H. Funakubo, K. Saito, J. Mater. Res. **16**, 303 (2001)
17. H.N. Lee, D. Hesse, Appl. Phys. Lett. **80**, 1040 (2002)
18. A. Garg, Z.H. Barber, M. Dawber, J.F. Scott, A. Snedden, P. Lightfoot, Appl. Phys. Lett. **83**, 2414 (2003)